Broadband and polarization-independent arbitrary ratio integrated optical power splitter built on thick silicon nitride platform*

ZHENG Langteng, CHEN Yiqiang, XUE Zhengqun, HUANG Jiwei, ZHU Minmin, and WANG Linghua**
College of Physics and Information Engineering, Fuzhou University, Fuzhou 350108, China

(Received 21 November 2023; Revised 8 April 2024)

Integrated optical power splitters are basic but indispensable on-chip devices in silicon photonics. They can be used either for power distribution or monitoring, or as the building blocks for more complex devices or circuits. Although different types of optical power splitters with different architectures have been proposed and demonstrated, devices that could work with arbitrary power splitting ratio in a large bandwidth without polarization dependence are still rare to be seen. In this paper, we propose and investigate an optical power splitter with adiabatically tapered waveguide structures on a thick silicon nitride platform, which could meet the requirement mentioned above. With optimized structural parameters obtained by three-dimensional finite-difference time-domain (3D-FDTD) simulation, the polarization dependence of different power splitting ratio gets almost eliminated for each specific working wavelength. In a broad wavelength range (1 340—1 800 nm), the insertion loss (*IL*) of the device is below 1 dB, and the variation of the power splitting ratio (*PSR*) can be controlled within ~±5% if compared with the targeted design value for 1 550 nm centered wavelength. Simple structure, relaxed critical dimensions, and good fabrication tolerance make this device compatible with the standard fabrication process in commercial silicon photonic foundries.

Document code: A **Article ID:** 1673-1905(2024)10-0577-7
DOI https://doi.org/10.1007/s11801-024-3258-3

Silicon photonics (SiPh) has become a promising solution for the realization of high-density photonics integrated circuits (PICs) in large volume, leveraging its seamless compatibility with complementary metal oxide semiconductors (CMOS) technique[1]. Among various on-chip devices in SiPh, optical power splitters (OPSs) are basic but indispensable ones, being used in scenarios where power distribution or monitoring are required[2,3]. They are also the building blocks for more complex devices or circuits, such as Mach-Zehnder modulators, optical phased arrays (OPAs), switches or sensors[4-7]. To date, different types of OPSs with different architectures have been proposed and demonstrated, mostly on the popular silicon-on-insulator (SOI) platform, which include directional couplers (DCs)[8,9], Y-branches[10,11], multimode interference (MMI) couplers, subwavelength gratings (SWGs) or metamaterials[12,13]. DCs can be used to obtain different power splitting ratios (*PSRs*) easily in low insertion loss (*IL*), but they are susceptible to wavelength, polarization states and fabrication errors. MMIs can offer larger bandwidth, but their *IL* values are normally high. Y-branches and SWGs are also available choices, but they require more stringent fabrication control for their feature sizes. Meanwhile, some of these available OPSs only support a fixed *PSR*, which limit their applications. Noticeably, it is still very challenging for OPSs in SiPh to simultaneously have all these characteristics mentioned above, namely, compactness, low-loss, large operational bandwidth, polarization-independence, easy tailorable *PSR*, and ideally, being readily fabricated with available commercial foundry facilities.

As an alternative in SiPh, the SiN platform has emerging as a promising platform for photonics integration[14,15]. Besides of the several advantages offered by the material itself, the relatively lower refractive index of SiN combining with the continuous efforts paid on the fabrication process optimization, enable the waveguide losses in SiN to be substantially reduced to a very low point, which is important for passive devices like OPSs, or large-scale circuits like OPAs. Meanwhile, the large fabrication tolerance releases the stress on the side of both design and fabrication. Furthermore, SiN can be processed by back-end-of-line (BEOL) processes, by which multilayer structures such as SiN-on-SOI can be realized[16]. They would help to diversify the functionalities of the

* This work has been supported by the Fujian Provincial Department of Science and Technology (No.2022I0006), the Natural Science Foundation of Fujian Province (No.2020J01467), and the National Natural Science Foundation of China (No.61405198).
** WANG Linghua is an associate professor at the College of Physics and Information Engineering, Fuzhou University. He received his Ph.D. degree in 2013 from Dalian University of Technology. His research interests are mainly in integrated photonics. E-mail: linghua.wang@fzu.edu.cn

multilayer photonic chip together with high integration density.

As its thickness increases, SiN film tends to crack because of the intrinsically high film stress during the deposition, especially by the process such as low-pressure chemical vapor deposition (LPCVD). But recently, this problem has been circumvented by different optimized fabrication processes, e.g. mechanical trenches or Damascene technique[17,18]. Hence, the height of the SiN can be customized, facilitating numerous new applications. For example, the waveguide can be engineered to have either negative or positive dispersion, which is essential for Kerr frequency comb or super-continuum generation applications[19]. This freedom in the waveguide dimension also endows the design of the SiN-based passive devices with much more flexibility.

In this paper, we propose and investigate an OPS with adiabatically tapered waveguide structures on a thick SiN platform. Although the overall structure is simple, we found the device can meet nearly all the requirements discussed above. In particularly, not only the *PSR* at the two outputs of the device could be tailored arbitrarily by adjusting the structure parameters, but also under these different *PSRs*, the device works almost without polarization dependence. In a broad wavelength range (1 340—1 800 nm), the *IL* of the device is below 1 dB, and the variation of the *PSR* can be controlled within ~±5% if compared with the targeted design value for 1 550 nm centered wavelength.

The schematic of proposed OPS in SiN material is shown in Fig.1, which includes one input waveguide and two output ones. The function of power splitting is realized mainly by its coupling region, which is consisted of one central tapered waveguide and two inverted tapered ones placed on each side, with the gap separation of G_1 and G_2, respectively. The light propagating in the input waveguide will get less confined when it is gradually tapered from a width of W_1 to a tip width of W_2, along a coupling length L. To a point where phase matching condition is met, the power will be coupled from the central tapered waveguide to the two side-placed inverted tapered waveguides. Then S-bend waveguides with the same width of W_1 are used to decouple and route the light to the output ports. All the waveguides are strip ones, with silicon dioxide (SiO_2) as the bottom- and top-cladding.

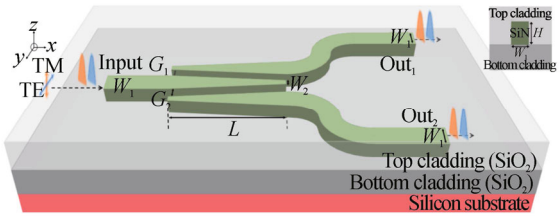

Fig.1 Schematic of the proposed OPS (Inset: cross-section of the strip SiN waveguide)

OPSs with similar structure has been proposed previously on either silicon or SiN platform[20,21]. A distinct advantage of OPSs built with this structure is that not only equal *PSR* (50: 50) can be realized by a symmetry structure (G_1=G_2) with low *IL*, but different *PSRs* can also be tailored continuously, simply by fixing one gap, G_1, while changing the other one, G_2, accordingly, thus making the structure asymmetric (G_1≠G_2). However, a challenge commonly faced by the devices demonstrated so far is that most of them work with a high polarization dependance. Because of the different electric-field discontinuity condition at the tapered coupling region, the *PSR* designed for transverse-electric (TE) polarization at a specific central wavelength can hardly work the same for the transverse-magnetic (TM) polarization, or vice versa, except of the equal splitting case (50: 50). Meanwhile, even for one polarization only, the *PSR* would also deviate from the targeted designing value when the working wavelength is changed, mostly because of the waveguide dispersion. The superposition of these effects makes the performance of the available devices built with the proposed structure far from satisfactory, which is thirstily desired to achieve arbitrary polarization-independent *PSRs* in a large bandwidth. But according to our study, this problem can be well solved by taking the thickness of the waveguide into account and re-optimizing the structure parameters.

Three-dimensional finite-difference time-domain (3D-FDTD) solver from Ansys, Inc. is used to optimize the structure throughout the process, and the dispersions of the materials are considered. Waveguide height H, waveguide width W_1, and coupling length L are three key structural parameters that need to be optimized. Firstly, we calculate the dependence of the *PSRs* and *ILs* of a series of OPSs on the wavelengths under three different waveguide heights, which are H=400 nm, 800 nm, and 1 200 nm. On SiN platform, H=400 nm represents waveguides with moderate confinement, while H=800 nm and 1 200 nm represent waveguides with high confinement. In all cases, G_1 and W_2 are kept constant as 200 nm in order to satisfy the minimal fabrication resolution requirement of the available SiPh foundry, where 193 nm or 248 nm deep ultraviolet (DUV) lithography is used[1,22]. And the radius of the S-bend waveguide is chosen as 60 μm to minimize its impact on the bending loss. W_1 and L are initially set as 800 nm and 65 μm, respectively. Then G_2 is carefully adjusted to achieve *PSR* of 90: 10, 80: 20, 70: 30, 60: 40, and 50: 50 for 1 550 nm central wavelength. The results are shown in Fig.2 and Fig.3. As can be seen from Fig.2, for the OPSs designed with H=400 nm, obviously the obtained *PSR* values are both polarization- and wavelength-dependent, except of the 50: 50 case. For example, at 1 550 nm wavelength, the *PSR* value changes from the targeted 70: 30 in TE polarization to 62: 38 in TM polarization. Meanwhile, for TE polarization only, the *PSR* values change from targeted 70: 30 to 76: 24 and 63: 37 when

the working wavelength changes to 1 350 nm and 1 750 nm, respectively. Switching to TM polarization at these two wavelengths would further exacerbate the *PSR* difference. Nevertheless, it is clearly that increasing of the waveguide height would help to alleviate the wavelength dependance of *PSR* values under each targeted designing one, and make the *PSR* values in two polarizations close to each other at the same time. As for both polarizations, the *PSR* values on the side of longer wavelengths increases, and those on the side of shorter wavelengths decrease when *H* is increased. Hence the slopes of the curves decrease overall. The influence of *H* on *IL* is also quite significant. As can be seen from Fig.3, for both polarizations, *ILs* can be drastically reduced on the side of longer wavelengths. But the *ILs* on the side of shorter wavelengths would be larger if *H* is increased from 800 nm further to 1 200 nm.

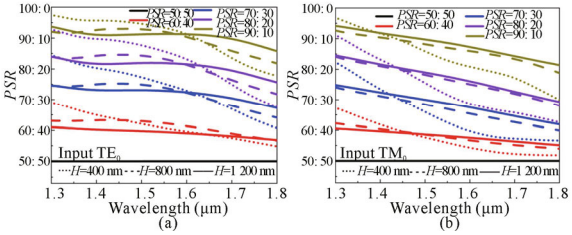

Fig.2 *PSRs* as a function of wavelength in 1 300—1 800 nm for two polarizations, where different *H* values are considered: (a) TE polarization; (b) TM polarization

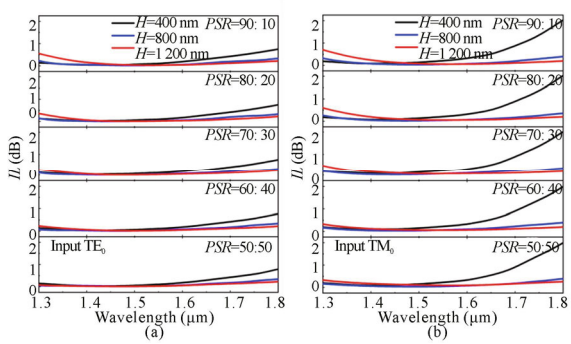

Fig.3 *ILs* as a function of wavelength for two polarizations, where different *PSR* and *H* values are considered: (a) TE polarization; (b) TM polarization

In the next, we investigate the influences of W_1 on the performance of the proposed OPS, the results are shown in Fig.4 and Fig.5. In this calculation, *H* is fixed at 1 200 nm, and *L* remains the same as above. As can be seen, the increase of W_1 would help to further reduce the dependance of *PSR* values on the wavelengths under each targeted designing one, and the impact is more significant in TM polarization (Fig.4). However, as W_1 gets larger, the *ILs* on the side of shorter wavelengths will dramatically increase (Fig.5). This is because with shorter wavelengths and larger W_1, higher order modes tend to be excited in the coupling region that is close to the end of the input port, which would result in higher transmission loss. Hence W_1 should not be too large, and W_1=800 nm is an appropriate value considering both the OPS and *IL* in a broad bandwidth.

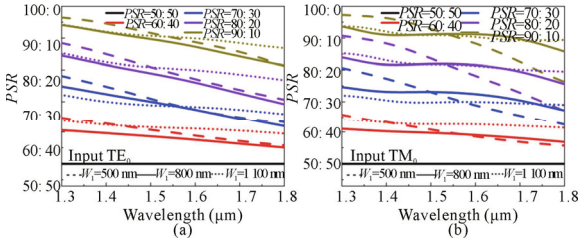

Fig.4 *PSRs* as a function of wavelength in 1 300—1 800 nm for two polarizations, where different W_1 values are considered: (a) TE polarization; (b) TM polarization

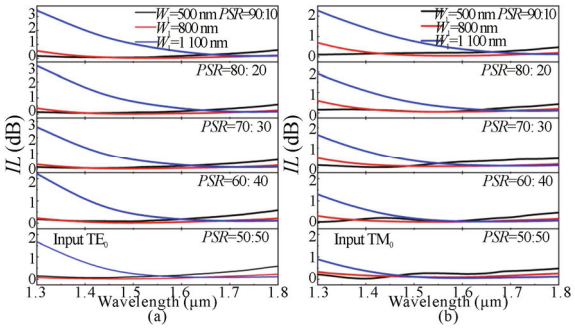

Fig.5 *ILs* as a function of wavelength for two polarizations, where different *PSR* and W_1 values are considered: (a) TE polarization; (b) TM polarization

The last structural parameter we optimized is *L*. The results are shown in Fig.6 and Fig.7. In contrast to *H* and W_1, the influence of *L* on the *PSRs* of the device is relatively limited. However, the increasing of *L* would help to reduce the *ILs* of the OPSs, especially on the side of shorter wavelengths. The choice of *L* value can be balanced between *IL* and the compactness of the device.

Based on the device optimization presented above, the main design structural parameters of the proposed OPS are chosen to be: H=1 200 nm, W_1=800 nm, W_2=200 nm, G_1=200 nm, and L=40 μm. Corresponding to *PSR* of 90: 10, 80: 20, 70: 30, 60: 40, and 50: 50 at 1 550 nm central wavelength, G_2 are 300 nm, 350 nm, 410 nm, 480 nm, and 590 nm, separately. Under these conditions, the characteristics of proposed OPS can be substantially improved, and the results are shown in Fig.8 and Tab.1. In the wavelength range considered (1 300—1 800 nm), the polarization dependence of the *PSR* value gets almost eliminated for each specific working wavelength. Meanwhile, compared with each targeted designing *PSR* value for 1 550 nm centered wavelength, the variation of *PSR* can be controlled within ~±5% in such a large bandwidth. And in the full wavelength range, the *ILs* of the designed OPS can be almost suppressed all below 1 dB for different *PSR* values both in two polarizations

except the case of 90: 10, for which the wavelength range satisfying *IL*<1 dB is 1 340—1 800 nm. The electric field intensity distribution of the device working under different *PSR*s in two polarizations at 1 550 nm are presented in Fig.9, which confirms the functional reliability of the proposed device. It is noted that we also closely check the optimized results for the device with H=800 nm and W_2=300 nm (not shown here). And it seems that our device is quite robust only if the waveguides still fall within high confinement regime (H>800 nm). The performance would deteriorate only a bit with the reduction of H from 1 200 nm to 800 nm (*PSR* variation is within ~±7% if compared with the targeted design value for 1 550 nm centered wavelength in the full wavelength range), which would help to release the difficulty of fabrication to a certain extent. Good performance of the device can also be obtained when W_2 is relaxed to 300 nm, but at the cost of its footprint. L needs to be increased from 40 μm to 65 μm for the *IL* reduction. Limited by our hardware conditions for numerical simulations, in practice, more extensive calculations can be conducted on a supercomputer, with advanced optimization algorithm (e.g. particle swarm optimization) in combined with, to obtain further optimized results with more fine structure parameters[23].

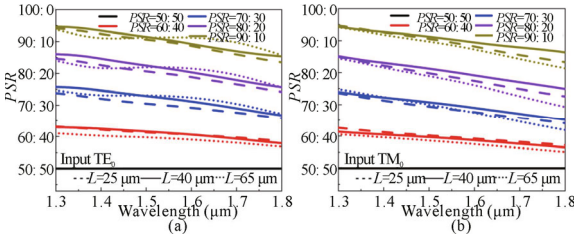

Fig.6 *PSRs* as a function of wavelength in 1 300—1 800 nm for two polarizations, where different *L* values are considered: (a) TE polarization; (b) TM polarization

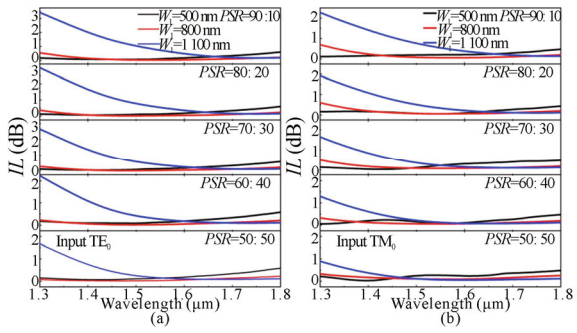

Fig.7 *ILs* as a function of wavelength for two polarizations, where different *PSR* and *L* values are considered: (a) TE polarization; (b) TM polarization

Finally, we evaluate the fabrication tolerance of the proposed device by changing the waveguide width and height. The former would also cause the variation of the gap separation, G_1 and G_2, accordingly, which were taken into account during the calculation. For brevity but without generality, only the results for the targeted designing *PSR* of 70: 30 are presented, as shown in Fig.10. The results for the other *PSRs* are similar. Because the tapered waveguide structures are adopted in the coupling region, our device exhibit large tolerance to fabrication errors. For the variation of W_1 within ±40 nm, the variation of *PSR* at each specific working wavelength is nearly below 3.5% for both polarizations in the full wavelength range. The worst case is for TE polarization at 1 300 nm, where the *PSR* is 72.6: 27.4 for ΔW=−40 nm and 78.1: 21.9 for ΔW=+40 nm. The *IL* can almost be kept well below 1 dB, except the case of TM polarization at 1 300 nm, which would surpass 1 dB once the W_1 deviates larger than 10 nm in the negative direction. But it is still less than 1.5 dB. The variation of H within ±40 nm has little influence on the *PSR* and *IL* within the wavelength range of 1 300—1 800 nm.

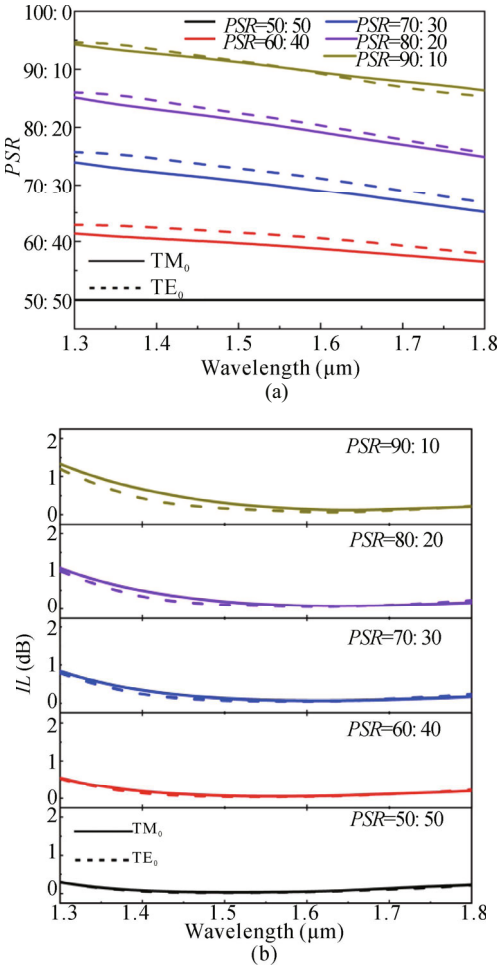

Fig.8 Characteristics of the optimized device in a broad bandwidth: (a) Different *PSRs* in two polarizations; (b) *ILs* under different *PSRs* for two polarizations

A comparison of the previously reported OPSs with ours is given in Tab.2. As can be seen, OPSs that can achieve arbitrary polarization-independent *PSRs* in an

ultra-large bandwidth are still very few. For Ref.[29], it was achieved by a rather complex sandwich waveguide structure, where the refractive index of the SiN_x layer sandwiched between the silicon layer is required to be tuned. Compared with that, our device is completely compatible with available SiPh foundries. There are no extremely small features which are challenging for the fabrication.

Tab.1 *PSR* values of the optimized device under three working wavelengths (1 300 nm, 1 550 nm, and 1 800 nm) for two polarizations

Aimed *PSR* (%)	G_2 (nm)	*PSR* @1 300 nm	*PSR* @1 550 nm	*PSR* @1 800 nm
50: 50	300	50.0: 50.0 (TE) 50.0: 50.0 (TM)	50.0: 50.0 (TE) 50.0: 50.0 (TM)	50.0: 50.0 (TE) 50.0: 50.0 (TM)
60: 40	350	62.9: 37.1 (TE) 61.4: 38.6 (TM)	60.1: 39.9 (TE) 59.4: 40.6 (TM)	57.9: 42.1 (TE) 56.5: 43.5 (TM)
70: 30	410	75.7: 24.3 (TE) 74.0: 26.0 (TM)	71.6: 28.4 (TE) 69.4: 30.6 (TM)	66.8: 33.2 (TE) 65.1: 34.9 (TM)
80: 20	480	86.0: 14.0 (TE) 85.2: 14.8 (TM)	81.2: 18.8 (TE) 80.0: 20.0 (TM)	75.7: 24.3 (TE) 74.9: 25.1 (TM)
90: 10	590	94.6: 5.4 (TE) 94.3: 5.7 (TM)	90.3: 9.7 (TE) 90.2: 9.8 (TM)	85.4: 14.6 (TE) 86.4: 13.6 (TM)

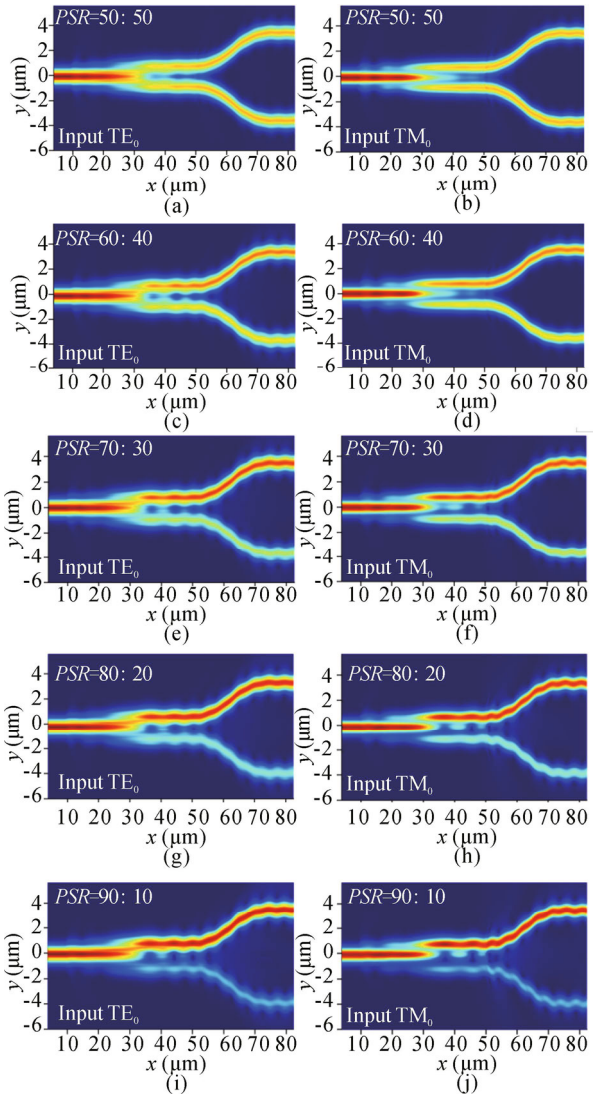

Fig.9 Electric field intensity distributions of the device working under different *PSRs* in two polarizations at 1 550 nm

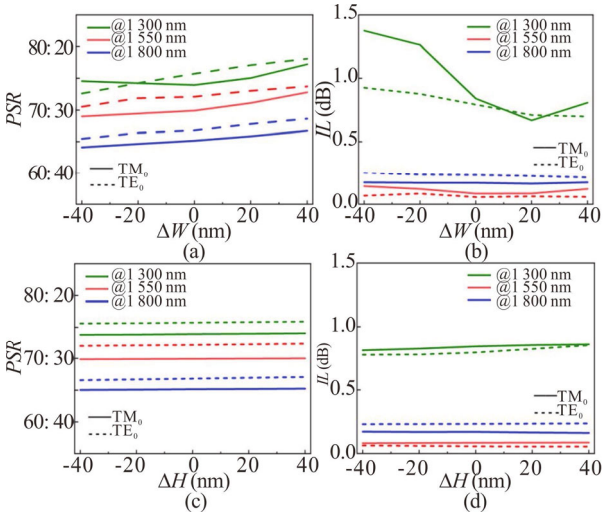

Fig.10 Calculated fabrication tolerance of the device to the deviation of waveguide width W_1 and thickness H under three working wavelengths (1 300 nm, 1 550 nm, and 1 800 nm) for two polarizations: (a) *PRS* vs. ΔW; (b) *IL* vs. ΔW; (c) *PRS* vs. ΔH; (d) *IL* vs. ΔH

In conclusion, we propose and investigate an OPS with adiabatically tapered waveguide structures on a thick SiN platform, which could work with arbitrary power splitting ratio in a large bandwidth without polarization dependence. With optimized structural parameters obtained by 3D-FDTD simulation, the polarization dependence of different *PSRs* get almost eliminated for each specific working wavelength. In a broad wavelength range (1 340—1 800 nm), the *IL* of the device is below 1 dB under different *PSR* values, and the variation of the *PSR* can be controlled within ~±5% if compared with the targeted design value for 1 550 nm centered wavelength. Simple structure, relaxed critical dimensions, and good fabrication tolerance make this device compatible with the standard fabrication process of commercial silicon photonic foundries.

Tab.2 Comparison between the reported optical power splitters and this work

Ref.	Platform	Structure	Feature size (nm)	Coupling length (μm)	*BW* (nm)	Max *IL* in *BW* (dB)	Different *PSR*	Polarization-independent *PSR*
[24]	SOI	SWG-assisted asymmetric directional coupler	110	5.25	300	0.33	No	No
[25]	SOI	Parameterized Y-junction	200	2.32	100	0.36	Yes	No
[26]	SOI	Adiabatic tapers with SWG	110	2.125	520	0.2	No	No
[27]	SOI	Adiabatic coupler	150	200	100	1.0	Yes	No
[28]	SOI	Partially shallowly etched MMI	100	5.8	560	0.4	No	Yes
[29]	Si: SiN: Si	Sandwich adiabatic tapers	100	7	100	0.31	Yes	Yes
[21]	SIN	Adiabatic tapers	100	80	100	0.02	Yes	No
[30]	SiN	Modal-engineered slot waveguide	200	260	420	0.62	No	Yes
This work	SiN	Adiabatic tapers with thick SIN waveguides	200	40	460	1.0	Yes	Yes

Ethics declarations

Conflicts of interest

The authors declare no conflict of interest.

References

[1] SIEW S Y, LI B, GAO F, et al. Review of silicon photonics technology and platform development[J]. IEEE journal of lightwave technology, 2021, 39(13): 4374-4389.

[2] SUN J, TIMURDOGAN E, YAACOBI A, et al. Large-scale nanophotonic phased array[J]. Nature, 2013, 493: 195-199.

[3] CHRISTOPHER R D, NICOLAS K F, LAWRENCE L B. PDM-DQPSK silicon receiver with integrated monitor and minimum number of controls[J]. IEEE photonics technology letters, 2012, 24(8): 697-699.

[4] XU M, CAI X. Advances in integrated ultra-wideband electrooptic modulators[J]. Optics express, 2022, 30(5): 7253-7274.

[5] LIU L, LIU N, ZHANG J, et al. High performance electro-optic modulator based on thin-film lithium niobate[J]. Optoelectronic letters, 2022, 18(10): 0583-0587.

[6] SUN J, TIMURDOGAN E, YAACOBI A, et al. Large-scale silicon photonic circuits for optical phased arrays[J]. IEEE journal of selected topics in quantum electronics, 2014, 20(4): 264-278.

[7] WANG R, VASILIEV A, MUNEEB M, et al. III-V-on-silicon photonic integrated circuits for spectroscopic sensing in the 2–4 μm wavelength range[J]. Sensors, 2017, 17(8): 1788.

[8] CHEN X, LIU W, ZHANG Y, et al. Polarization-insensitive broadband 2×2 3 dB power splitter based on silicon-bent directional couplers[J]. Optics letters, 2017, 42(19): 3738-3740.

[9] GUPTA R K, CHANDRAN S, DAS B K. Wave length-independent directional couplers for integrated silicon photonics[J]. Journal of lightwave technology, 2017, 35(22): 4916-4923.

[10] GOUDARZI K, KIM D, LEE H, et al. Ultra low loss broadband 1×2 optical power splitters with various splitting ratios[J]. Optics continuum, 2022, 1(9): 1888-1895.

[11] TAO S H, FANG Q, SONG J F, et al. Cascade wide-angle Y-junction 1×16 optical power splitter based on silicon wire waveguides on silicon-on-insulator[J]. Optics express, 2008, 16(26): 21456-21461.

[12] RUIZ J L P, ALDAYA I, DAINESE P, et al. Design of compact arbitrary-ratio multimode power splitters based on topological derivative[J]. IEEE photonics technology letters, 2020, 32(18): 1187-1190.

[13] SHIRAN H, LIBOIRON-LADOUCEUR O. Dual-mode broadband compact 2×2 optical power splitter using sub-wavelength metamaterial structures[J]. Optics express, 2021, 29(15): 23864-23876.

[14] XIANG C, JIN W, BOWERS J E. Silicon nitride passive and active photonic integrated circuits: trends and prospects[J]. Photonics research, 2022, 10(6): A82-A96.

[15] MUÑOZ P, MICÓ G, BRU L A, et al. Silicon nitride photonic integration platforms for visible, near-infrared and mid-infrared applications[J]. Sensors, 2017, 17(9): 2088.

[16] WANG L, PENG H, ZHENG L, et al. Broadband and CMOS-compatible polarization splitter and rotator built on a silicon nitride-on-silicon multilayer platform[J]. Applied optics, 2023, 62(4): 1046-1056.

[17] LUKE K, DUTT A, POITRAS B C, et al. Overcoming Si_3N_4 film stress limitations for high quality factor ring resonators[J]. Optics express, 2013, 21(19): 22829-22833.

[18] PFEIFFER H P M, LIU J, RAJA S A, et al. Ultra-smooth silicon nitride waveguides based on the Damascene reflow process: fabrication and loss origins[J]. Optica, 2018, 5(7): 884-892.

[19] PORCEL A G M, SCHEPERS F, EPPING P J, et al. Two-octave spanning supercontinuum generation in stoichiometric silicon nitride waveguides pumped at telecom wavelengths[J]. Optics express, 2017, 25(2): 1542-1554.

[20] NGUYEN V H, KIM I K, SEOK T J. Low-loss and broadband silicon photonic 3-dB power splitter with enhanced coupling of shallow-etched rib waveguides[J]. Applied sciences, 2020, 10(13): 4507.

[21] ZHU J, CHAO Q, HUANG H, et al. Compact, broadband, and low-loss silicon photonic arbitrary ratio power splitter using adiabatic taper[J]. Applied optics, 2021, 60(2): 413-416.

[22] WILMART Q, EL DIRANI H, TYLER N, et al. A versatile silicon-silicon nitride photonics platform for enhanced functionalities and applications[J]. Applied sciences, 2019, 9(2): 255.

[23] ZHANG B, CHEN W, WANG P, et al. Particle swarm optimized polarization beam splitter using metasurface-assisted silicon nitride Y-junction for mid-infrared wavelengths[J]. Optics communications, 2019, 451: 186-191.

[24] YE C, DAI D. Ultra-compact broadband 2×2 3 dB power splitter using a subwavelength-grating-assisted asymmetric directional coupler[J]. Journal of lightwave technology, 2020, 38(8): 2370-2375.

[25] LIN Z, SHI W. Broadband, low-loss silicon photonic Y-junction with an arbitrary power splitting ratio[J]. Optics express, 2019, 27(10): 14338-14343.

[26] WANG Z, LIU Y, WANG Z, et al. Ultra-broadband 3 dB power splitter from 1.55 to 2 μm wave band[J]. Optics letters, 2021, 46(17): 4232-4235.

[27] MAO D, WANG Y, EL-FIKY E, et al. Adiabatic coupler with design-intended splitting ratio[J]. Journal of lightwave technology, 2019, 37(24): 6147-6155.

[28] CHEN Y, XIAO J. Ultracompact and broadband silicon-based polarization-independent 1×2 power splitter using a shallowly etched multimode interference coupler[J]. Journal of the optical society of America B, 2021, 38(10): 3064-3070.

[29] WANG J, LIU H, ZHANG Y, et al. Study on polarization-independent optical power splitter with designable splitting ratio[J] Laser & optoelectronics progress, 2023, 60(17): 1723001.

[30] GONZÁLEZ-ANDRADE D, GUERBER S, DURÁN-VALDEIGLESIAS E, et al. Ultra-wideband dual-polarization silicon nitride power splitter based on modal engineered slot waveguides[J]. Optics letters, 2020, 45(2): 527-530.